# Efficient molecular organic light-emitting diodes based on silole derivatives

Leonidas C. Palilis,[a‡] Antti J. Mäkinen,[a] Hideyuki Murata,[b] Manabu Uchida,[c] and Zakya H. Kafafi[a]†

[a]Optical Sciences Division, U.S. Naval Research Laboratory, Washington, DC 20375

[b]School of Materials Science, Japan Advanced Institute of Science Technology, Ishikawa 923-1292, Japan

[c]Chisso Corporation, Yokohama, Kanagawa 236-8605, Japan

[‡]Also at SFA Inc., Largo, MD 20774; electronic mail: leonidas@ccs.nrl.navy.mil

†Electronic-mail: kafafi@ccf.nrl.navy.mil

## Abstract

We report the performance of molecular organic light-emitting diodes (MOLEDs) using silole derivatives as emissive and electron transport materials. Two siloles, namely 2,5-di-(3-biphenyl)-1,1-dimethyl-3,4-diphenylsilacyclopentadiene (PPSPP) and 1,2-bis(1-methyl-2,3,4,5,-tetraphenylsilacyclopentadienyl)ethane (2PSP), with high PL quantum yields of 94% and 85%, respectively, were used as emissive materials. Another silole, namely 2,5-bis-(2',2"-bipyridin-6-yl)-1,1-dimethyl-3,4-diphenylsilacyclopentadiene (PyPySPyPy), was used as the electron transport material. MOLEDs using these two siloles and NPB as the hole transport material show a low operating voltage of approximately 4.5 V at a luminance of 100 cd/m$^2$ and high external electroluminescence (EL) quantum efficiencies of 3.4% and 3.8%, respectively, at 100 A/m$^2$. MOLEDs based on PPSPP exhibit a red-shifted EL spectrum which is assigned to an exciplex formed at the PPSPP:NPB interface.



Organic Light-Emitting Materials and Devices VI, Zakya H. Kafafi, Homer Antoniadis, Editors, Proceedings of SPIE Vol. 4800 (2003) © 2003 SPIE · 0277-786X/03/$15.00

# Report Documentation Page

*Form Approved*
*OMB No. 0704-0188*



| 1. REPORT DATE | 2. REPORT TYPE | 3. DATES COVERED |
|---|---|---|
| **2003** | | **00-00-2003 to 00-00-2003** |

| 4. TITLE AND SUBTITLE | 5a. CONTRACT NUMBER |
|---|---|
| **Efficient molecular organic light-emitting diodes based on silole derivatives** | 5b. GRANT NUMBER |
| | 5c. PROGRAM ELEMENT NUMBER |
| 6. AUTHOR(S) | 5d. PROJECT NUMBER |
| | 5e. TASK NUMBER |
| | 5f. WORK UNIT NUMBER |
| 7. PERFORMING ORGANIZATION NAME(S) AND ADDRESS(ES) **Naval Research Laboratory,4555 Overlook Avenue SW,Washington,DC,20375** | 8. PERFORMING ORGANIZATION REPORT NUMBER |
| 9. SPONSORING/MONITORING AGENCY NAME(S) AND ADDRESS(ES) | 10. SPONSOR/MONITOR'S ACRONYM(S) |
| | 11. SPONSOR/MONITOR'S REPORT NUMBER(S) |

12. DISTRIBUTION/AVAILABILITY STATEMENT
**Approved for public release; distribution unlimited**

13. SUPPLEMENTARY NOTES

14. ABSTRACT

15. SUBJECT TERMS

| 16. SECURITY CLASSIFICATION OF: | | | 17. LIMITATION OF ABSTRACT | 18. NUMBER OF PAGES | 19a. NAME OF RESPONSIBLE PERSON |
|---|---|---|---|---|---|
| a. REPORT **unclassified** | b. ABSTRACT **unclassified** | c. THIS PAGE **unclassified** | | **15** | |

## Introduction

Significant progress in the field of molecularly based organic light-emitting diodes (MOLEDs) has been made since the first report of Tang *et. al.* [1]. The design of new emissive and charge transport molecular materials has resulted in high performance MOLEDs that are rapidly approaching the high standards required for display applications. [2-4] Presently, the device performance is limited by the low electron mobilities and the small solid state electron affinities of the electron transporting materials since most organic molecules preferentially transport holes. The development of stable electron transport materials is therefore a challenge that has been the focus of intense research over the last few years. The hole and electron transporting molecules N,N'-diphenyl-N,N'-bis (3-methylphenyl)-1,1'-biphenyl-4,4'diamine (TPD) and tris-(8-hydroxyquinoline) aluminum ($Alq_3$), commonly used in MOLEDs, have hole and electron mobilities that differ by a factor of ~1000 (~$10^{-3}$ $cm^2$/Vsec and ~$10^{-6}$ $cm^2$/Vsec, respectively). [5,6] Electron transport in most organics is dispersive [7], which results in high operating voltages and subsequent device degradation. In addition to the widely used electron transporter $Alq_3$, [8] derivatives of nathrolines, [7] oxadiazoles, [9] quinolines, [10] quinoxalines, [11] and benzothiadiazoles [12] have also been used. Electron mobilities on the order of $10^{-4}$-$10^{-3}$ $cm^2$/Vsec, mostly dispersive, have been reported in an inert atmosphere. [7,11,12]

The development of highly emissive materials with large solid state photoluminescence (PL) quantum yields [13] represents another challenge. Intermolecular interactions usually dominant in the solid state result in luminescence quenching and a smaller PL efficiency relative to the molecular quantum yield. Recently, silole derivatives have been proposed as a new class of electron transport and highly fluorescent materials. [14-18] Siloles have large electron affinities due to the $\sigma^*$-$\pi^*$ conjugation arising from the interaction between the $\sigma^*$ orbital of the two exocyclic Si-C $\sigma$-bonds on the silole ring and the $\pi^*$ orbital of the butadiene moiety. [14,15] This interaction results in lowering the position of the lowest unoccupied molecular orbital (LUMO). A recent study by Murata *et. al.* on a silole derivative, namely 2,5-bis-(2',2''-bipyridin-6-yl)-1,1-dimethyl-3,4-diphenylsilacyclopentadiene (PyPySPyPy), shows that it exhibits non-dispersive electron transport with a high mobility of $2x10^{-4}$ $cm^2$/Vsec at 0.64 MV/cm in either nitrogen or air. [16] Using PyPySPyPy in the electron transport layer and a highly luminescent silole derivative, namely 1,2-bis(1-methyl-2,3,4,5,-tetraphenylsilacyclopentadienyl)ethane (2PSP) in the emissive layer with a TPD hole transporting layer, an EL quantum efficiency of 4.8% was measured at 100 A/$m^2$. [17] Here, we report the performance of MOLEDs using 2PSP and a new blue, highly fluorescent silole derivative, namely 2,5-di-(3-biphenyl)-1,1-dimethyl-3,4-diphenylsilacyclopentadiene (PPSPP) as emissive materials with PyPySPyPy and N,N'-diphenyl-N,N'-(2-napthyl)-(1,1'-phenyl)-4,4'-diamine (NPB) as the electron and hole

transporting materials, respectively. A low operating voltage of ~4.5 V was measured at a luminance of 100 cd/$m^2$ and high external EL quantum efficiencies of 3.4% and 4% were obtained at ~100A/$m^2$ for PPSPP and 2PSP, respectively.

**Experimental details**

The silole derivatives were synthesized by an one-step process from bis(phenylethynyl)silanes based on the intermolecular reductive cyclization followed by the palladium-catalyzed cross-coupling with aryl halide. [15] They were purified by recrystallization, column chromatography and vacuum sublimation. They form amorphous polycrystalline films upon vacuum evaporation with relatively high glass transition temperatures (~ 85°C). The chemical structures of the silole derivatives used in this study are depicted in Figure 1.

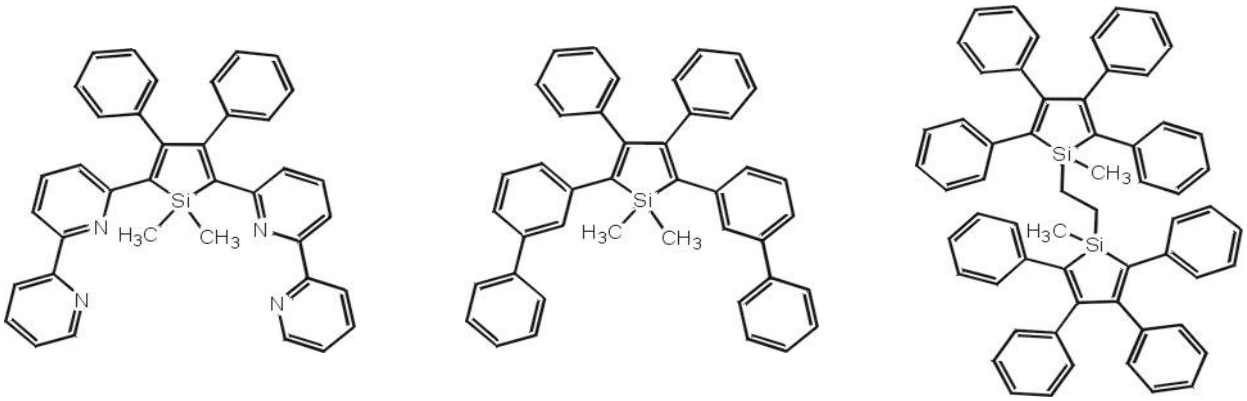


PyPySPyPy PPSPP 2PSP

**Figure 1**. Chemical structures of silole derivatives.

Multilayer light-emitting diodes were prepared in a vacuum chamber at a pressure of ~5x$10^{-7}$ Torr. Indium tin oxide (ITO) patterned glass substrates were precleaned and treated with an oxygen plasma. A 50 nm thick film of NPB was first deposited onto ITO. This was followed by the deposition of a 60 nm thick film of one of the silole derivatives: PPSPP, 2PSP, PyPySPyPy as the emissive and electron transport layer. In three-layer devices, a 10 nm thick film of PyPySPyPy was used only as the electron transport layer (ETL) with an additional 50 nm thick film of PPSPP or 2PSP as the emitting layer (EML). The total thickness of the organic layers was estimated to be 110 nm. The deposition rate was measured using a quartz crystal microbalance and used to estimate the total thickness of the deposited layers. A 150-nm thick Mg:Ag (15:1 ratio by weight) film was used as the cathode. Details about the device characterization techniques can be found elsewhere. [17,18] Ultraviolet photoemission spectroscopy (UPS) and X-ray photoemission spectroscopy (XPS) were carried out using an

Omicron Multiprobe UHV system (base pressure ~$10^{-10}$ Torr) that consists of a preparation and an analysis chamber separated by a gate valve. 2PSP, PPSPP and PyPySPyPy were deposited onto a 10 nm thick vapor-deposited Ag film. For the Mg-on-PyPySPyPy interface, Mg was evaporated onto a 10 nm thick organic film. UPS spectra were recorded using HeI (hν=21.22 eV) and HeII (hν=40.82eV) radiation. XPS spectra were recorded for Al*Ka* radiation (hν=1486.6 eV). The resolution of the analyzer was ~50 meV for the UPS and ~1 eV for the XPS measurements.

## Results and Discussion

### I. Spectroscopic characterization of the silole derivatives

Polycrystalline films of PPSPP, 2PSP and PyPySPyPy exhibit blue, greenish blue and green fluorescence, respectively. The absolute PL quantum yields of thin films of 2PSP, PPSPP and PyPySPyPy were measured using an integrating sphere in a $N_2$ atmosphere and are (94±5)%, (85±5)% and (28±3)%, respectively. The PL quantum yields of 2PSP and PPSPP are among the highest reported for neat organic films. Upon substitution of the phenyl group of PPSPP with the electron withdrawing bipyridyl group, the PL efficiency of PyPySPyPy decreases to 28%. Figure 2 shows the PL spectra of NPB, PyPySPyPy and NPB:PyPySPyPy (molar ratio 1:1) composite films and the EL spectrum of a bilayer device with PyPySPyPy as the EML/ETL.

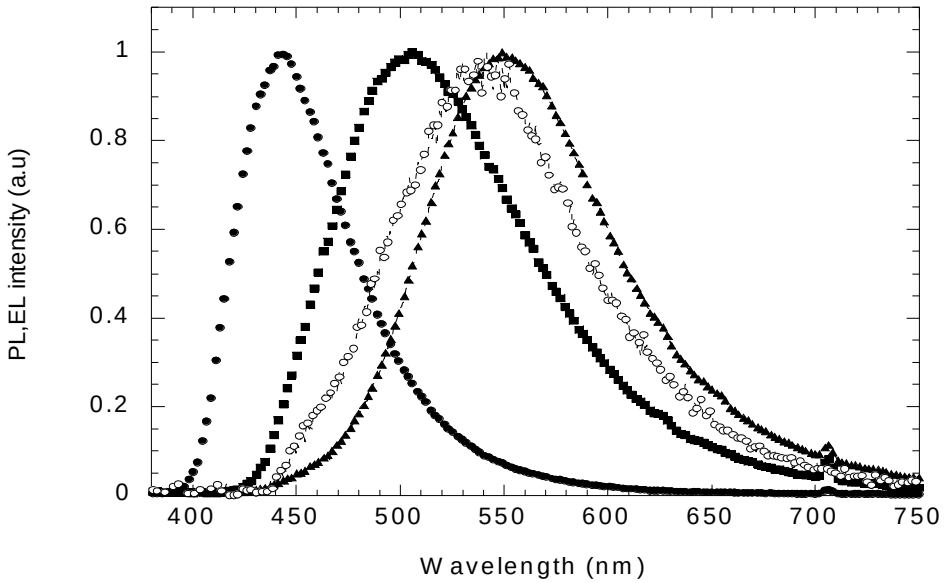


**Figure 2**. PL spectra of NPB (closed circles), PyPySPyPy (closed squares), NPB:PyPySPyPy (closed triangles) and EL spectrum of a MOLED with PyPySPyPy as EML/ETL (open circles).

The PL spectra of NPB, PPSPP and NPB:PPSPP composite films, along with the EL spectra of bilayer devices with a PPSPP EML/ETL and three-layer devices with PPSPP and PyPySPyPy as the EML and ETL, respectively, are shown in Figure 3.

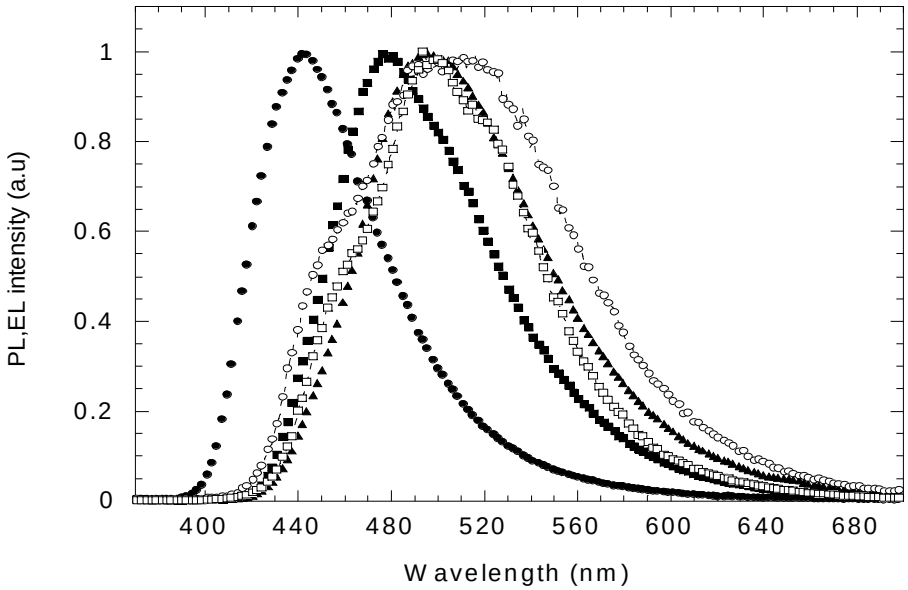


**Figure 3**. PL spectra of NPB (closed circles), PPSPP (closed squares), NPB:PPSPP (molar ratio 1:1) (closed triangles) and EL spectra of bilayer (open circles) and three-layer (open squares) devices with PPSPP as EML/ETL and PPSPP and PyPySPyPy as EML and ETL, respectively.

The PL spectrum of PPSPP shows blue emission with a peak at 475 nm. The peak emission of PyPySPyPy is at 505 nm, showing a 30 nm red shift relative to that of PPSPP. Substitution of the phenyl with the electron withdrawing bipyridyl group seems to result in an increase in the π-electron delocalization in PyPySPyPy and its red-shifted emission spectrum. The PL spectra of composite films of NPB and PyPySPyPy or NPB and PPSPP are red-shifted relative to those of neat films of PyPySPyPy and PPSPP. The PL spectrum of the NPB:PyPySPyPy composite film has a peak at 550 nm, red-shifted by 45 nm relative to that of PyPySPyPy. Similarly, the PL spectrum of the NPB:PPSPP composite film is centered at 495 nm, red-shifted by 20 nm relative to PPSPP. These red-shifted PL spectra are attributed to excited state complexes (exciplexes) formed between NPB and PPSPP or PyPySPyPy, respectively. [18] The EL spectra of the bilayer and three-layer devices are similar to those of the composite film PL spectra confirming the formation of an exciplex at the interface between NPB and PPSPP or PyPySPyPy. The weak shoulder around 450 nm in the EL spectra of the bilayer devices is due to a contribution from NPB which indicates that electron-hole recombination partially occurs inside

NPB. Indirect carrier recombination may take place between NPB and PPSPP or PyPySPyPy resulting in the formation of an exciplex with a red-shifted featureless EL spectrum. Exciplex formation is favored due to the large difference between the energy levels of the HOMO and LUMO of the two molecules (see next section). [20] The absolute PL quantum yields of the NPB:PPSPP and NPB:PyPySPyPy films were measured and are ~ 62% and 21%, respectively. [18] The PL quantum efficiencies of both exciplexes are slightly lower than those of the respective siloles suggesting that the lifetimes of the silole excited states and those of the corresponding exciplexes are similar. [19] It is worth noting that the PL quantum yield of NPB:PPSPP is the highest reported for exciplex emission. Figure 4 shows the PL spectrum of 2PSP and the EL spectrum of a device with a 2PSP emissive layer.

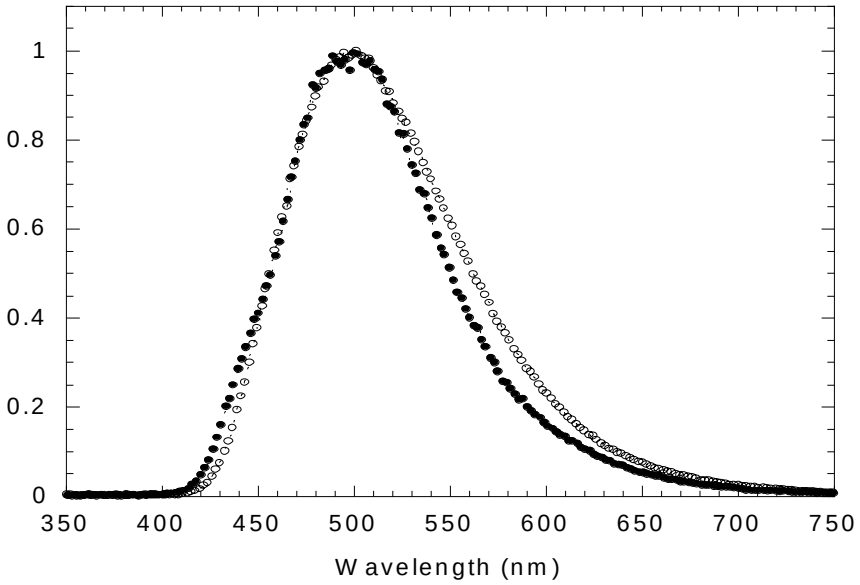


**Figure 4**. PL spectrum of 2PSP (open squares) and EL spectrum of bilayer devices based on 2PSP as the emissive/electron transport layer (closed circles).

The PL and EL spectra of 2PSP are almost identical exhibiting an emission maximum at around 495 nm which indicates that the same excited state is formed both under photoexcitation and carrier injection. No evidence for exciplex formation between NPB and 2PSP was found, which is difficult to understand considering the similar energetics between NPB and PPSPP, PyPySPyPy or 2PSP (see next section).

## II. Ultraviolet and X-Ray photoemission studies

### a) Energy level alignment at the Ag/Silole Interfaces

Figure 5 shows the energy level diagrams of the three siloles deduced from the UPS study.

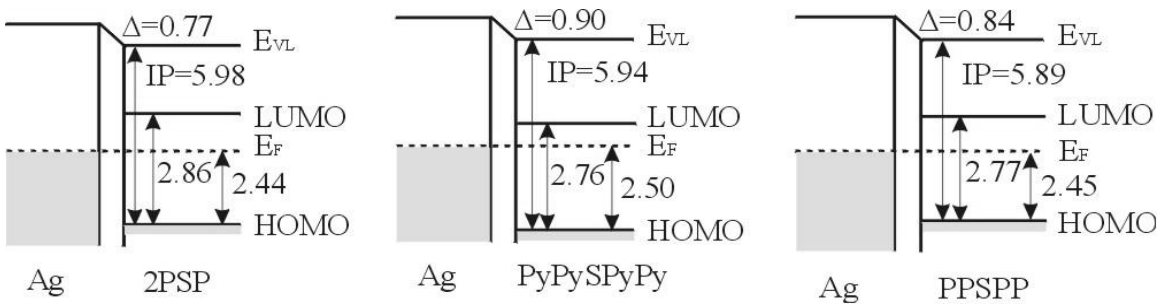


**Figure 5**. Energy level alignment at the metal-organic interface as determined by UPS. Δ is the vacuum level shift between the metal and the organic. The LUMO-HOMO separation reflects the optical bandgap determined from the absorption onset. All energies are given in electron volts.

Upon deposition of one of the siloles on Ag, an abrupt shift of the vacuum level (VL) is observed which is completed at ~16 Å Ag coverage. This shift of 0.77 eV, 0.90 eV and 0.84 eV, is assigned to interface dipoles forming at the Ag/2PSP, Ag/PyPySPyPy and Ag/PPSPP interfaces, respectively. The vacuum level shift results in the lowering of the LUMO level of the siloles relative to the Fermi level of Ag, i.e. a decrease in the barrier to electron injection (LUMO-$E_F$). The ionization potentials were determined from the position of the HOMO relative to the siloles' VL and have similar values for the three siloles, namely ~5.94 eV for PyPySPyPy, ~5.89 eV for PPSPP and ~5.98 eV for 2PSP. This suggests that the HOMO level is mainly located on the silole ring and is not much influenced by the substituents on the silole ring. The estimated LUMO-Fermi level separation was slightly different for the three siloles, namely ~0.26 eV for PyPySPyPy, ~0.32 eV for PPSPP and ~0.42 eV for 2PSP. The LUMO level is slightly lowered upon substitution of the phenyl group with the electron withdrawing bipyridyl group, indicating that a smaller barrier to electron injection occurs at the Ag/PyPySPyPy interface.

### b) Energy level alignment at the Mg/PyPySPyPy Interface

The electronic structure at the interface between PyPySPyPy and Mg was studied using UPS and XPS. Figures 6a and 6b show the evolution of the Mg(1s) and N(1s) core levels as a function of Mg coverage on PyPySPyPy. Each peak was fitted with one or two Gaussians.

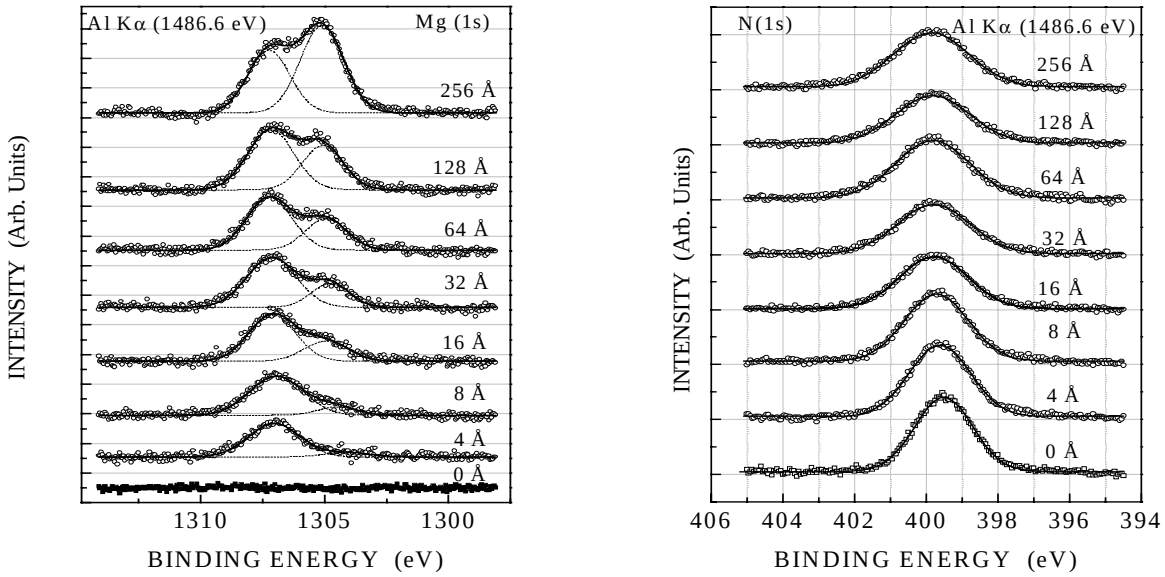


**Figure 6**. (a) Mg(1s) and (b) N(1s) core levels as a function of Mg coverage on PyPySPyPy.

Following the initial Mg deposition (4 Å), the Mg(1s) core level spectrum consists of a high binding energy (BE) peak at 1307.2 eV. With increasing Mg coverage (above 16 Å) a low BE peak appears at 1305.1 eV that grows further upon Mg deposition and dominates the spectra for coverages above 256 Å. The low BE peak is assigned to a neutral Mg species that accumulates on top of PyPySPyPy with increasing coverage, while the high BE peak represents fully or partially oxidized Mg signaling electron transfer from Mg to PyPySPyPy. The net chemical shift of the Mg(1s) core level is +2.1 eV (shift to higher BE), accounting for the shift of the vacuum and Fermi levels. The total area below the Mg(1s) peaks increases with increasing Mg coverage. The N(1s) core level exhibits a net -0.25 eV shift to lower BE. Similarly, the C(1s) and the Si(2s) levels (not shown here) undergo shifts to lower BEs of -0.25 eV and -0.8 eV, respectively. [22] The shifts of all the core levels to lower BEs indicate an addition of a negative charge on PyPySPyPy, consistent with the picture of electron transfer from Mg to PyPySPyPy. The C(1s) level also exhibits some broadening upon Mg deposition with an increase of FWHM close to 0.6 eV. A strong chemical interaction between Mg and PyPySPyPy may contribute to this broadening. [23]

## III. Device characterization

Figures 7 and 8 compare the current-luminance-voltage characteristics of bilayer devices using either PyPySPyPy or PPSPP or 2PSP as the EML/ETL.

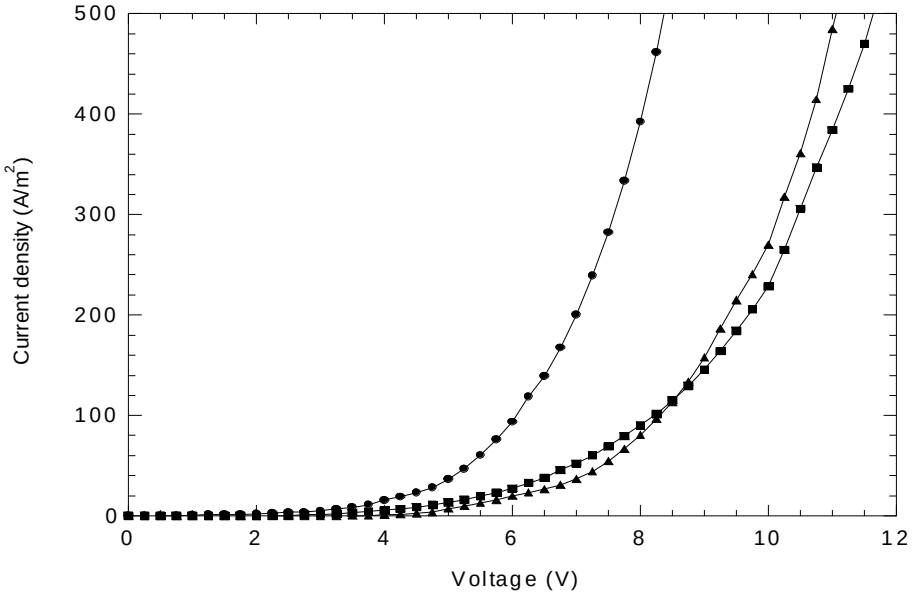


**Figure 7.** Current density versus voltage characteristics for devices with a PyPySPyPy (closed circles), a PPSPP (closed squares) and a 2PSP (closed triangles) emissive/electron transport layer.

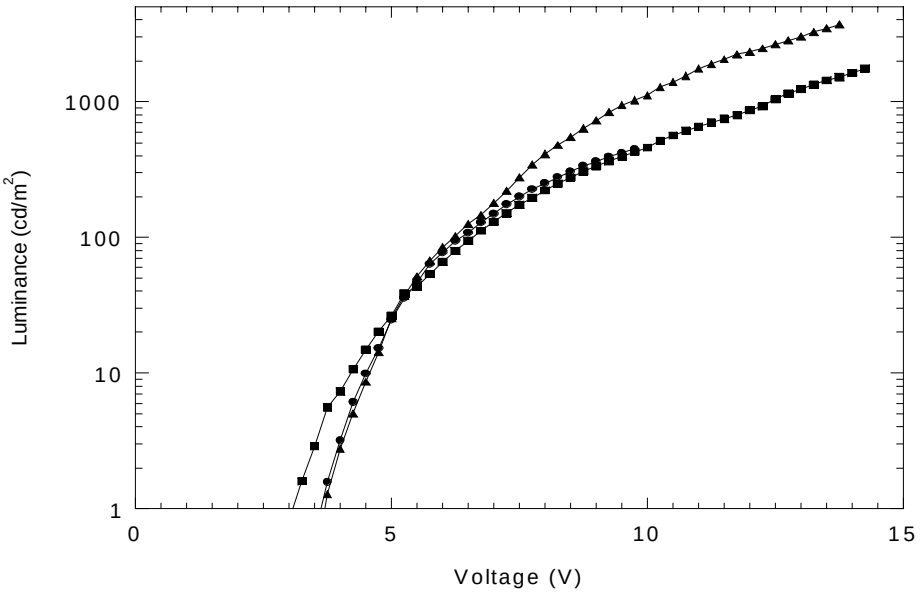


**Figure 8**. Luminance versus voltage characteristics for devices with a PyPySPyPy (closed circles), a PPSPP (closed squares) and a 2PSP (closed triangles) emissive/electron transport layer.

Bilayer devices using PyPySPyPy as the ETL/EML show a significantly higher current density at the same voltage compared to those using PPSPP or 2PSP as the emissive/ETL layer. Based on the results of the UPS studies of the Ag/silole interfaces, the electron injection barriers are only slightly different for the three siloles (with PyPySPyPy showing the lowest barrier). Assuming similar results (very similar values for the electron injection barriers of the three siloles) at the Mg:Ag/silole interface, the very low turn on and operating voltages of the PyPySPyPy based devices cannot be attributed mainly to the difference in the electron injection barriers. Rather, better electron transport in PyPySPyPy compared to PPSPP and 2PSP has to be invoked to explain the above behavior. In multilayer MOLEDs, as the current voltage characteristics are influenced by the injection and transport of both electrons and holes, better electron transport is expected to result in a lower device operating voltage. By employing the time-of-flight technique, Murata *et. al.* has found that PyPySPyPy exhibits non-dispersive electron transport with a weak electric-field dependence. A high mobility of $2x10^{-4}$ $cm^2$/Vsec was measured at 0.64 MV/cm. [16] The lower operating voltage of the devices with PyPySPyPy as the ETL/EML can thus be attributed to the high electron mobility of PyPySPyPy as well as the slightly lower injection barrier for electron injection to PyPySPyPy from the Mg:Ag cathode as is inferred from the UPS measurements on the Ag/silole interfaces.

Electron-only devices based on PyPySPyPy with symmetric Mg:Ag contacts also exhibit a higher electron current flow compared to 2PSP and PPSPP suggesting a higher conductivity for the PyPySPyPy molecule. [24] This result may also suggest that PyPySPyPy is a better electron transport material with a higher electron mobility compared to 2PSP and PPSPP (assuming very similar values for the electron injection barriers of the three siloles at the Mg:Ag silole interfaces). The higher electron conductivity of PyPySPyPy relative to the other two siloles may be due to the presence of the strong electron withdrawing bipyridyl moieties. The small dipole moment of PyPySPyPy is also thought to reduce energetic disorder thus resulting in a higher (non-dispersive) electron mobility [16]. All bilayer devices show similar turn on voltages. As the injection and transport of electrons will mainly dictate the luminance turn on voltage for these devices, the similarity between the turn on voltages for the three devices suggests that the electron transfer rate at the NPB/silole interface is similar for the three siloles. 2PSP devices show the highest luminance of 3850 cd/$m^2$ compared to 1725 cd/$m^2$ for PPSPP and 475 cd/$m^2$ for PyPySPyPy devices.

In Figure 9, a comparison of the EL quantum efficiencies of these devices as a function of current density is presented.

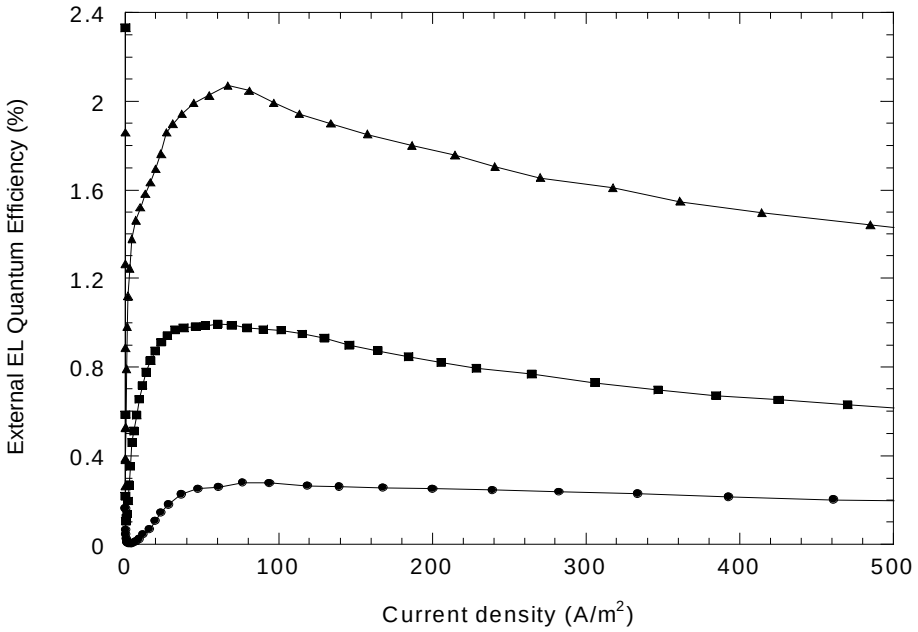


**Figure 9.** EL quantum efficiency as a function of current density for devices with a PyPySPyPy (closed circles), a PPSPP (open circles) and a 2PSP (closed triangles) EML/ETL.

2PSP shows a maximum EL quantum efficiency of 2.2% compared to 1% for PPSPP and 0.3% for PyPySPyPy (at ~100 A/m$^2$). The trend for the device quantum efficiencies qualitatively follows the trend of the PL quantum yields of the siloles. The most efficient silole (2PSP) shows the best device performance while the least efficient silole (PyPySPyPy) shows the worse device performance. However, the ratio of PL and EL efficiencies for 2PSP (~0.023) is a factor of ~2 larger than those of PPSPP (0.012) and PyPySPyPy (0.011), which are nearly the same. Exciplex formation at the PPSPP or PyPySPyPy/NPB interface as well as different electron injection/hole transfer rates and exciton recombination/quenching rates may also contribute to the lower device performance when PPSPP and PyPySPyPy is used as the ETL/EML.

Figure 10 compares the luminance-voltage characteristics of three-layer devices using PPSPP or 2PSP as the EML and PyPySPyPy as the ETL. Figure 11 shows the external EL quantum efficiency (ELQE) versus current density for these devices.

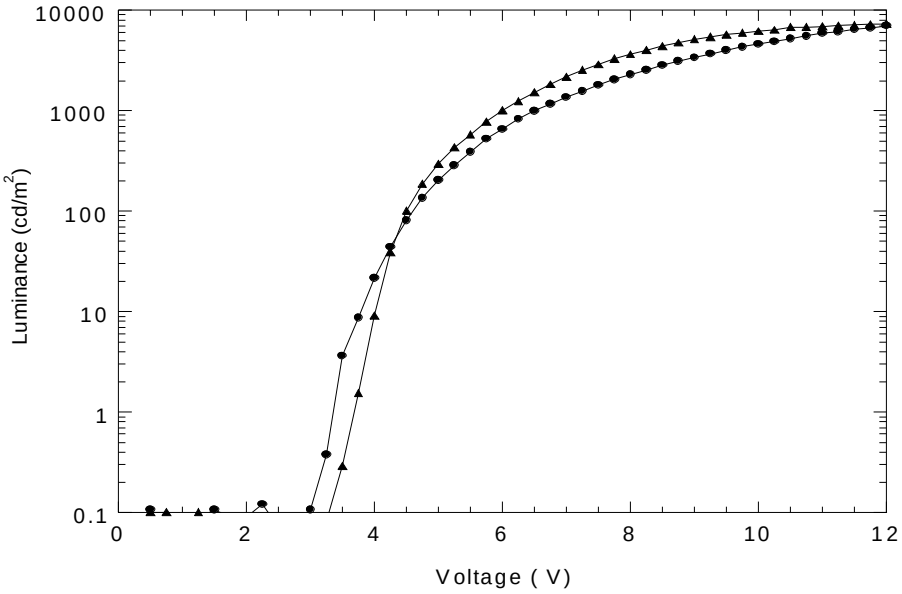


**Figure 10.** Luminance versus voltage for a) 2PSP/PyPySPyPy emissive/electron transport bilayer (closed circles) b) PPSPP/PyPySPyPy emissive/electron transport bilayer (closed triangles).

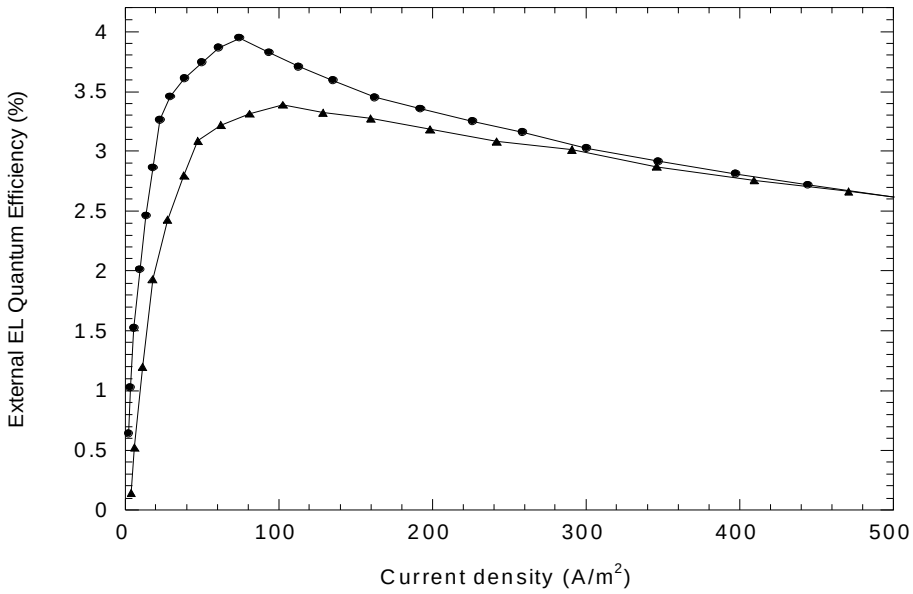


**Figure 11.** ELQE versus current density for a) 2PSP/PyPySPyPy emissive/electron transport bilayer (closed circles) b) PPSPP/PyPySPyPy emissive/electron transport bilayer (closed triangles).

Three layer devices using PyPySPyPy as the ETL and 2PSP or PPSPP as the EML exhibit a lower turn-on and operating voltage compared to bilayer devices using 2PSP or PPSPP as the ETL/EML. These three layer devices also exhibit very similar current density-voltage characteristics compared to the bilayer devices with PyPySPyPy as the emissive/ETL layer. Since the current voltage characteristics strongly depend on the injection and transport of electrons, an excellent electron transporter with a low-lying LUMO level (PyPySPyPy) adjacent to the cathode that results in a small electron injection barrier will facilitate electron injection and transport to the emissive silole layer. The alignment of the silole LUMO levels is further expected to facilitate electron transfer at the 2PSP or PPSPP/PyPySPyPy interface. Three layer devices also show much higher luminances compared to the bilayer devices. Luminances of 100 cd/m$^2$ are achieved at 4.5 and 4.6 V for PPSPP and 2PSP devices, respectively. A luminance of 1000 cd/m$^2$ was obtained at 6 V for PPSPP and 6.5 V for 2PSP. In comparison, bilayer devices with a 2PSP, PPSPP or a PyPySPyPy emissive/electron transport layer reach a luminance of 100 cd/m$^2$ at 6.0, 6.6 and 6.35 V, respectively. The much higher luminance values observed in the three-layer devices are attributed to the higher exciton density and the better exciton confinement within the highly emissive 2PSP and PPSPP layers as a result of the improved electron injection/transport due to PyPySPyPy. Maximum luminances of 7000 to 9000 cd/m$^2$ were consistently achieved at 13 to 14 V for PPSPP and 2PSP three-layer devices. The corresponding EL quantum efficiency of the three-layer devices reaches a maximum of 4 and 3.4% for 2PSP and PPSPP, respectively (at ~100 A/m$^2$). At 1000 A/m$^2$, the quantum efficiencies are 2.1% for 2PSP and 2% for PPSPP. The corresponding power efficiencies of PPSPP devices are 4 and 5.2 lm/W at 100 and 1000 cd/m$^2$, respectively. For 2PSP devices, the power efficiencies are 4.8 lm/W at 100 cd/m$^2$ and 3.5 lm/W at 1000 cd/m$^2$. The significant improvement of the EL quantum efficiency in the three layer devices is mainly attributed to the improved electron transport of PyPySPyPy compared to PPSPP and 2PSP which reduces electron accumulation and nonradiative recombination with exciton quenching at the cathode. Efficient carrier recombination as a result of the improved electron-hole balanced injection and transport that is achieved in a three-layer device configuration also contributes to the improved device efficiencies. The high $\Phi_{PL}$ of the siloles also contribute to the high overall EL performance of the silole devices. A summary of the three-layer device characteristics is presented in Table I.

| **Emitting layer** | **Driving Voltage (V) (at 100 cd/m$^2$)** | **EL Quantum Efficiency (%) (at 100 A/m$^2$)** | **Power Efficiency (lm/W) (at 100 cd/m$^2$)** |
|---|---|---|---|
| **2PSP** | 4.6[a] | 3.8[c] | 4.8[a] |
| **PPSPP** | 4.5[a] | 3.4[c] | 4.0[a] |

**Table I**. Comparison of the driving voltages, EL quantum and luminous power efficiencies of three-layer devices with PPSPP and 2PSP as emitting layers. PyPySPyPy was used as ETL.

## Conclusions

In summary, we have reported the performance of highly efficient MOLEDs based on novel silole derivatives used as emissive and electron transporting materials. Three-layer devices with PPSPP and 2PSP as emissive layers and a trap-free electron transporting silole derivative exhibit low operating voltages of ~4.5 V and high EL quantum efficiencies of 3.4 and 4%, respectively, at ~100 A/m$^2$. PPSPP and PyPySPyPy were also found to form exciplexes with the hole transporting NPB molecule. The high device performance is attributed to the use of the high electron mobility PyPySPyPy derivative and the highly fluorescent PPSPP (and NPB:PPSPP exciplex) and 2PSP emitters.

## Acknowledgements

The authors thank the Office of Naval Research for financial support of this work.

## References

1. C. W. Tang and S. A. Van Slyke, *Appl. Phys. Lett.* **51**, 913 (1987).
2. S. A. Van Slyke, C. H. Chen, and C. W. Tang, *Appl. Phys. Lett.* **69**, 2160 (1996).
3. J. Shi and C. W. Tang, *Appl. Phys. Lett.* **70**, 1665 (1997).
4. F. Steuber, J. Staudigel, M. Stössel, J. Simmerer, A. Winnacker, H. Spreitzer, F. Weissörtel, and J. Salbeck, *Adv. Mater.* **12**, 130 (2000).
5. Y. Shen, M. W. Klein, D. B. Jacobs, J. C. Scott, and G. G. Malliaras, *Phys. Rev. Lett.* **86**, 3867 (2001).
6. G. G. Malliaras, Y. Shen, D. H. Dunlap, H. Murata, and Z. H. Kafafi, *Appl. Phys. Lett.* **79**, 2582 (2001).
7. S. Naka, H. Okada, H. Onnagawa, and T. Tsutsui, *Appl. Phys. Lett.* **76**, 197 (2000).
8. X. Zhou, J. He, L. S. Liao, M. Lu, Z. H. Xiong, X. M. Ding, X. Y. Hou, F. G. Tao, C. E. Zhou, and S. T. Lee, *Appl. Phys. Lett.* **74**, 609 (1999).
9. J. Bettenhausen, P. Strohriegl, W. Brutting, H. Tokuhisa, T. Tsutsui, *J. Appl. Phys.* **82**, 4957 (1997).
10. R. G. Kepler, P. M. Beeson, S. J. Jacobs, R. A. Anderson, M. B. Sinclair, V. S. Valencia, and P. A. Cahill, *Appl. Phys. Lett.* **66**, 3618 (1995).
11. M. Redecker, D. D. C. Bradley, M. Jandke, P. Strohriegl, *Appl. Phys. Lett.* **75**, 109 (1999).
12. A. J. Campbell, D. D. C. Bradley, and H. Antoniadis, *Appl. Phys. Lett.* **79**, 2133 (2001).
13. C. C. Wu, Y. T. Lin, H. H. Chiang, T. Y. Cho, C. W. Chen, K. T. Wong, Y. L. Liao, G. H. Lee, and S. M. Peng, *Appl. Phys. Lett.* **81**, 577 (2002).

14. K. Tamao, M. Uchida, T. Izumizawa, K. Furukawa, and S. Yamaguchi, *J. Am. Chem. Soc*. **118**, 11974 (1996).
15. S. Yamaguchi, T. Endo, M. Uchida, T. Izumizawa, K. Furukawa, and K. Tamao, *Chem. Eur. J*. **6**, 1683 (2000).
16. H. Murata, G. G. Malliaras, M. Uchida, Y. Shen, and Z. H. Kafafi, *Chem. Phys. Lett*. **339**, 161 (2001).
17. H. Murata, Z. H. Kafafi, and M. Uchida, *Appl. Phys. Lett. **80**, 189 (2002).*
18. L. C. Palilis, H. Murata, A. J. Mäkinen, M. Uchida, and Z. H. Kafafi, *Mat. Res. Soc. Proc.* In Press, 2002.
19. L. C. Palilis, A. J. Mäkinen, M. Uchida, and Z. H. Kafafi, Submitted to *Appl. Phys. Lett*.
20. K. Itano, H. Ogawa, and Y. Shirota, *Appl. Phys. Lett*. **85**, 636 (1999).
21. J. Kalinowski, M. Cocchi, P. Di Marco, and V. Fattori, *Chem. Phys. Lett*. **318**, 137 (2000).
22. A. J. Mäkinen, M. Uchida and Z. H. Kafafi, Submitted to *Appl. Phys. Lett*.
23. C. Shen, A. Kahn, and J. Schwartz, *J. Appl. Phys.* **89**, 449 (2001).
24. L. C. Palilis and Z. H. Kafafi (Unpublished data).